

Provided for non-commercial research and education use.  
Not for reproduction, distribution or commercial use.



This article appeared in a journal published by Elsevier. The attached copy is furnished to the author for internal non-commercial research and education use, including for instruction at the authors institution and sharing with colleagues.

Other uses, including reproduction and distribution, or selling or licensing copies, or posting to personal, institutional or third party websites are prohibited.

In most cases authors are permitted to post their version of the article (e.g. in Word or Tex form) to their personal website or institutional repository. Authors requiring further information regarding Elsevier's archiving and manuscript policies are encouraged to visit:

<http://www.elsevier.com/copyright>



## Controllable atomic layer deposition of one-dimensional nanotubular TiO<sub>2</sub>

Xiangbo Meng<sup>a</sup>, Mohammad Norouzi Banis<sup>a</sup>, Dongsheng Geng<sup>a</sup>, Xifei Li<sup>a</sup>, Yong Zhang<sup>a</sup>, Ruying Li<sup>a</sup>, Hakima Abou-Rachid<sup>b,\*</sup>, Xueliang Sun<sup>a,\*</sup>

<sup>a</sup> Department of Mechanical and Materials Engineering, The University of Western Ontario, London, ON N6A 5B8, Canada

<sup>b</sup> Defense Research & Development Canada–Valcartier, 2459 Boulevard PieXI Nord, Québec, QC G3 J 1X5, Canada

### ARTICLE INFO

#### Article history:

Received 4 September 2012

Received in revised form 7 November 2012

Accepted 24 November 2012

Available online 30 November 2012

#### Keywords:

Atomic layer deposition

Titanium oxide

Nanotubes

Anodic aluminum oxide

Carbon nanotubes

### ABSTRACT

This study aimed at synthesizing one-dimensional (1D) nanostructures of TiO<sub>2</sub> using atomic layer deposition (ALD) on anodic aluminum oxide (AAO) templates and carbon nanotubes (CNTs). The precursors used are titanium tetraisopropoxide (TTIP, Ti(OCH(CH<sub>3</sub>)<sub>2</sub>)<sub>4</sub>) and deionized water. It was found that the morphologies and structural phases of as-deposited TiO<sub>2</sub> are controllable through adjusting cycling numbers of ALD and growth temperatures. Commonly, a low temperature (150 °C) produced amorphous TiO<sub>2</sub> while a high temperature (250 °C) led to crystalline anatase TiO<sub>2</sub> on both AAO and CNTs. In addition, it was revealed that the deposition of TiO<sub>2</sub> is also subject to the influences of the applied substrates. The work well demonstrated that ALD is a precise route to synthesize 1D nanostructures of TiO<sub>2</sub>. The resultant nanostructured TiO<sub>2</sub> can be important candidates in many applications, such as water splitting, solar cells, lithium-ion batteries, and gas sensors.

© 2012 Elsevier B.V. All rights reserved.

### 1. Introduction

Since the delivery of carbon nanotubes (CNTs) in 1991 [1], there has been an ever-increasing amount of new nanoscale materials reported and they have shown exceptional physicochemical properties over their bulk counterparts as well. As a return, currently the quest on nanostructured substances for numerous applications is extraordinarily intensive. Among various nanostructures (e.g., nanoparticles, nanotubes, nanowires, nanorods, and nanofilms), tubular materials feature hollow entities and high surface-to-volume ratios of materials. This often leads to many unexpected benefits in applications. Besides CNTs, non-carbon nanotubes are also important for many areas. For example, nanotubular metal oxides are superior to other forms of nanomaterials including CNTs in sensing ability, photo catalytic activity, water photolysis efficiency, and photovoltaic behavior [2]. Thus, nanotubes of metal oxides attracted much attention over the past decade.

Among transition metal oxides, TiO<sub>2</sub> is one of the most investigated compounds in contemporary materials science [3], ascribed to its desirable properties. First of all, TiO<sub>2</sub> is distinguished by its chemical stability, corrosion-resistance, non-toxicity, abundance, and cheapness [4]. Furthermore, TiO<sub>2</sub> is functionally versatile as well, accounting for its extensive use in photocatalysis, water splitting, solar cells, lithium-ion batteries, fuel cells, gas sensors

and self-cleaning units. As a consequence, there is an account of thousands of papers about nanostructured TiO<sub>2</sub> in literature. In the case of TiO<sub>2</sub> nanotubes, their synthesis and applications have drawn great effort in earlier studies, as well documented by many reviews [3,5–17]. In general, anodization is the most widely used route for fabricating TiO<sub>2</sub> nanotubes, first reported in 2001 by Grimes and co-workers [18]. In a later time, Grimes et al. made a comprehensive review [5] on anodized TiO<sub>2</sub> nanotubes. Two other widely used methods are hydrothermal and template-assisted chemical approaches [6]. Besides the aforementioned methods, more recently there was an increasing awareness of atomic layer deposition (ALD), a vapor-phase deposition technique, for developing TiO<sub>2</sub> nanotubes [19–26].

ALD is a gas-solid thin film process credited to Suntola and co-workers [27]. Relying on two sequentially cyclic self-limiting half-reactions, ALD enables films to develop in a layer-by-layer mode on a substrate surface. Therefore, ALD can precisely control film deposition at the atomic level and provide films with excellent uniformity and conformality. Another remarkable benefit of ALD is its low deposition temperature (generally lower than 400 °C, even down to room temperature) compared to chemical vapor deposition, rendering ALD applicable for heat-sensitive substrates (such as polymer, and biomaterials). These characteristics distinguish ALD from solution-based and other vapor-phase routes (e.g., chemical and physical vapor deposition) and make ALD a facile but versatile tool for fabrication of various nanostructures. In the past decade, ALD gradually went into a fashion for nanotechnology, owing to its aforementioned superiorities. Currently ALD has expanded its uses from two-dimensional (2D) planar films to a

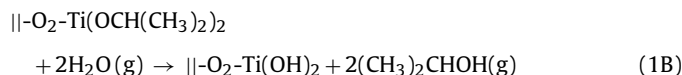
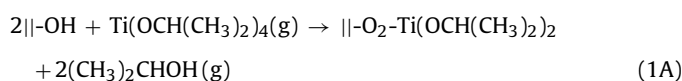
\* Corresponding authors.

E-mail addresses: [Hakima.Abou-Rachid@drdc-rddc.gc.ca](mailto:Hakima.Abou-Rachid@drdc-rddc.gc.ca) (H. Abou-Rachid), [xsun@eng.uwo.ca](mailto:xsun@eng.uwo.ca) (X. Sun).

variety of nanostructured materials, as recently reviewed [28–31]. Using ALD as the deposition tool, earlier researchers developed not only the aforementioned 1D nanotubes [19–26] but 2D planar films [32–40], 0D composite nanoparticles [41,42], and other complicated nanostructures [43,44] of TiO<sub>2</sub> as well. There are many precursors exposed in the previous studies of ALD-TiO<sub>2</sub>. TiCl<sub>4</sub> and titanium tetra-isopropoxide (TTIP, Ti(OCH(CH<sub>3</sub>)<sub>2</sub>)<sub>4</sub>) are two widely used titanium sources, and water is the most common oxygen source. In comparison, TTIP is more beneficial than TiCl<sub>4</sub>, for the induced ALD process has no release of the corrosive by-product HCl and no chlorine residues in the film [32,35].

Thanks to its inherent advantages, ALD profits the resultant nanostructures in many ways. In our recent work [44–47] it was demonstrated that ALD has the capability to control crystallinity of deposited metal oxides from amorphous to crystalline phase while it dominates film growth per cycle (GPC) and morphology. These intriguing characteristics of ALD make it possible to design nanomaterials with the desirable morphology as well as structural phase for specific applications. In this way, earlier studies posed a good example with ALD-V<sub>2</sub>O<sub>5</sub>. It was disclosed that ALD-induced amorphous V<sub>2</sub>O<sub>5</sub> showed better performance than widely used crystalline V<sub>2</sub>O<sub>5</sub> when they were used as cathode materials in lithium-ion batteries [48]. It was also revealed that ALD could further optimize V<sub>2</sub>O<sub>5</sub> cathodes by precisely controlling the deposited film thickness [48].

Stimulated by tremendous advantages of both 1D nanotubular structures and ALD, as discussed above, we attempted the synthesis of TiO<sub>2</sub> nanotubes by ALD using TTIP and water as precursors. The surface chemistry of ALD-TiO<sub>2</sub> has previously been investigated and the two half-reactions [34] induced by TTIP and water were described as follows:



In spite of the work [19–26,32–44] conducted previously with ALD-TiO<sub>2</sub>, our work features in two ways. First of all, two different substrates were used, i.e., porous anodic aluminum oxide (AAO) templates and CNTs. As a consequence, two different nanostructures were produced, i.e., pure TiO<sub>2</sub> nanotubes and CNT-TiO<sub>2</sub> coaxial tubular hybrids. In addition, another distinctive contribution is that the synthesized nanostructures showed structurally temperature-dependent crystallinity from amorphous to crystalline phase as well as tunable morphology. The synthesized TiO<sub>2</sub>-related nanostructures are potentially important candidates for many applications, as stated above.

## 2. Experimental

### 2.1. ALD-TiO<sub>2</sub>

In ALD-TiO<sub>2</sub> processes, commercial AAO (Whatman, Anodisc, 60 μm in thickness and 13 mm in diameter) and multi-walled CNTs (MWCNTs, Shenzhen Nanotech Port Co., Ltd., China) were first loaded into a commercial ALD reactor (Savannah 100, Cambridge Nanotechnology Inc., USA) preheated to a certain temperature. Then, TTIP (98%, Sigma-Aldrich) and deionized water (DI H<sub>2</sub>O) were introduced into the ALD reactor in an alternating sequence to perform ALD-TiO<sub>2</sub>. TTIP was heated to 70 °C while water was kept at room temperature in order to provide sufficient vapors for ALD-TiO<sub>2</sub> processes. Additionally, the delivery lines were heated

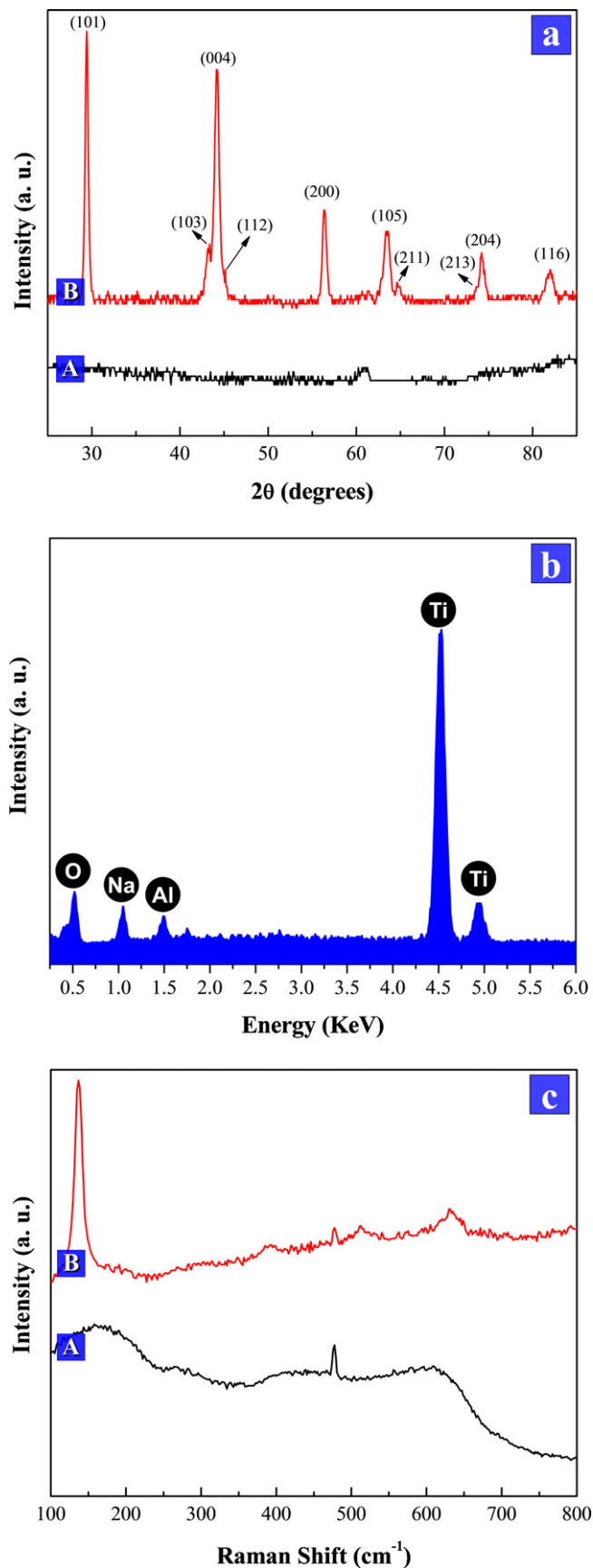
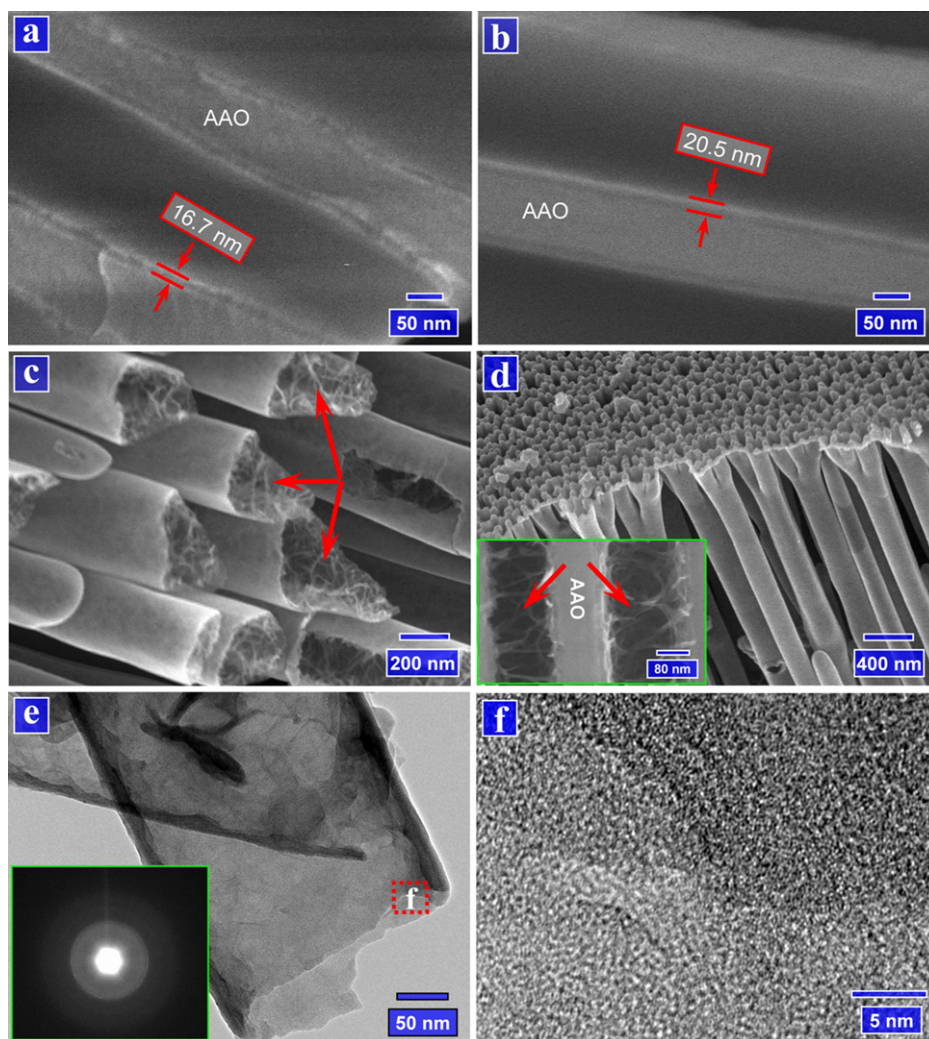


Fig. 1. (a) XRD patterns induced by ALD-TiO<sub>2</sub> on AAO at 150 °C (A) and 250 °C (B). (b) EDS spectrum of ALD-TiO<sub>2</sub> on AAO at 150 °C. (c) Raman spectra of ALD-TiO<sub>2</sub> on AAO at 150 °C (A) and 250 °C (B).



**Fig. 2.** Template-directed ALD-TiO<sub>2</sub> at 150 °C. SEM images showing AAO templates deposited with (a) 500- and (b) 600-cycle ALD-TiO<sub>2</sub>, and SEM images showing the received nanotubes arrays after (c) 500- and (d) 600-cycle ALD-TiO<sub>2</sub>. (e) TEM image of the received nanotubes (inset: SAED pattern). (f) HR-TEM image of a local area as marked with “f” in (e).

to 150 °C in order to prevent the precursors from condensation. Nitrogen was used as the carrier gas with a flow rate of 20 sccm and the ALD reactor was sustained at a low level of pressure (typically 0.4 Torr) with a vacuum pump (Pascal 2005 I, Adixon). The ALD procedures were set as follows: (1) a 1.0-s supply of TTIP; (2) a 3.0-s extended exposure of TTIP to AAO and CNTs; (3) a 10.0-s purge of oversupplied TTIP and any by-products; (4) a 2.0-s supply of water vapor; (5) a 3.0-s extended exposure of water vapor to AAO and CNTs; (6) a 10.0-s purge of oversupplied water and any by-products. The aforementioned six-step sequence constituted one ALD-TiO<sub>2</sub> cycle and the ALD processes could be adjustable with different cycling numbers and growth temperatures. In this study, two growth temperatures were employed for ALD-TiO<sub>2</sub> processes, i.e., 150 and 250 °C.

## 2.2. Functionalization of substrates

As is well-known, any ALD process requires functional groups with substrates in order to initiate the first deposition of target materials. Of the two substrates (AAO and CNTs), AAO as an oxide is generally covered by various functional groups (e.g., -OH) [49,50] and it has successfully been used in our previous work [47].

In contrast, CNTs are typically free of reactive sites due to their structural perfectness [51]. A general strategy for oxidation is

refluxing CNTs in nitric acid [52], and thereby functional groups (e.g., -OH) are created. In this study, the oxidation of CNTs was fulfilled using concentrated nitric acid (70% HNO<sub>3</sub>) in which CNTs were refluxed for 1–2 h at 100 °C. When the dispersions cooled down to room temperature, they were vacuum-filtered through a 0.2 μm membrane. The received CNTs were then washed by deionized water until a neutral pH value of the filtrate was received. The oxidized CNTs were dried in an oven at 100 °C overnight.

## 2.3. Strategies and resultant nanostructures

The commercial AAO is with numerous nanopores of nominal 200 nm while CNTs are nominally 60 nm in diameter. However, observation of using a field emission scanning electron microscope (FE-SEM, Hitachi 4800S) disclosed that the CNTs range widely from around 10 to over 100 nm, as shown by figure SI-1(a) and (b) in Supporting Information. In addition, it was found that acid treatment produced no observable change on the morphologies of CNTs (figure SI-1(c)–(f)).

Based on the two substrates, there are two different strategies induced by ALD and thereby the resultant TiO<sub>2</sub> shows different nanostructures. First of all, AAO-directed ALD-TiO<sub>2</sub> proceeds on the inner surfaces of AAO pores and therefore forms tubular films. Through dissolving AAO with 0.5 M sodium hydroxide (NaOH),

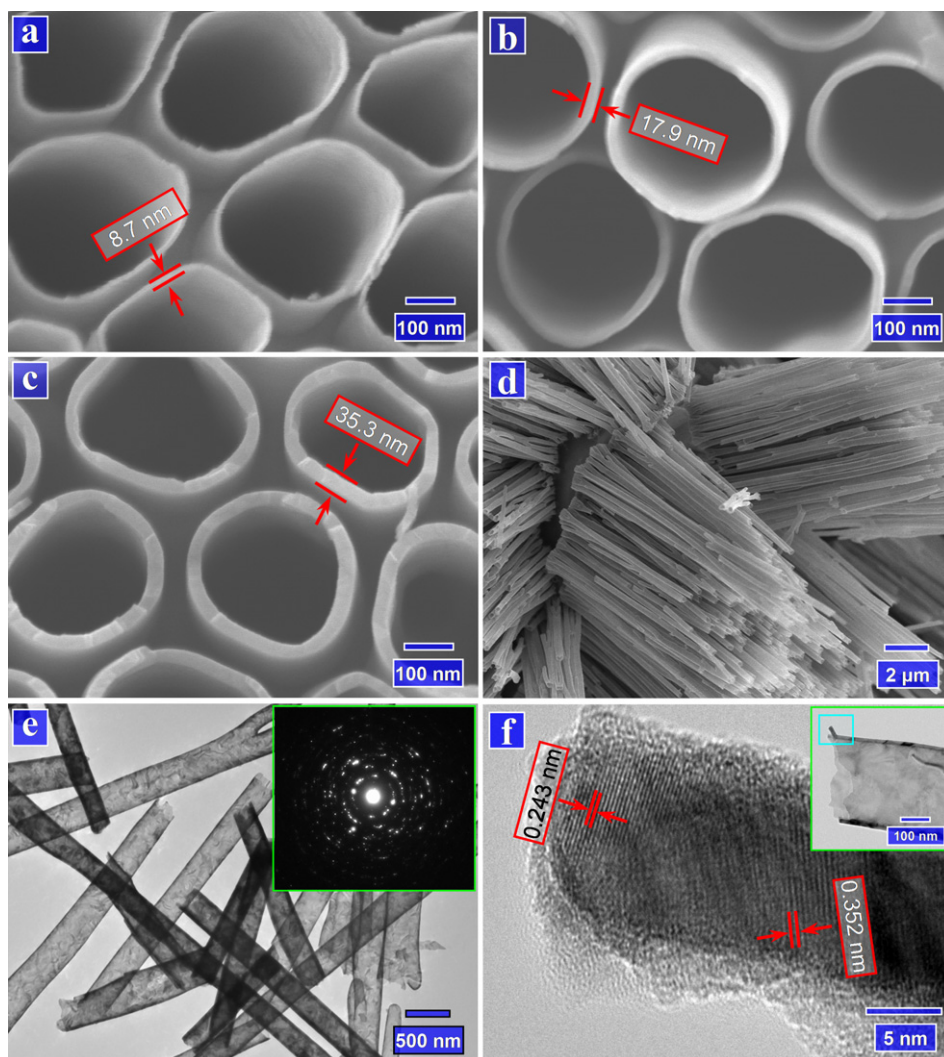


**Fig. 3.** Template-directed ALD-TiO<sub>2</sub> at 250 °C. SEM images showing AAO templates deposited with (a) 200- (b) 300-, and (c) 500-cycle ALD-TiO<sub>2</sub>. The received nanotubes shown by (d) SEM, (e) TEM (inset: SAED pattern), and (f) HR-TEM image (inset: the position for the piece examined by HR-TEM).

tubular films in nanopores of AAO are then released in forms of nanotubes. In comparison, CNT-based ALD-TiO<sub>2</sub> deposits films on the outer surfaces of CNTs. As a consequence, the outer films of TiO<sub>2</sub> construct coaxial tubular nanostructures with CNTs. In other words, the former strategy produces pure TiO<sub>2</sub> nanotubes while the latter yields CNT-TiO<sub>2</sub> coaxial tubular hybrids.

#### 2.4. Characterization

To characterize the morphologies, structures, and compositions of deposited materials, we used a FE-SEM (Hitachi 4800S) coupled with energy dispersive spectroscopy (EDS), transmission electron microscope (TEM, Hitachi 7000), high-resolution TEM (HR-TEM, JEOL 2010 FEG), X-ray diffractometer (XRD, Inel multi-purpose diffractometer), and Raman spectroscopy (HORIBA Scientific LabRAM HR).

### 3. Results and discussions

#### 3.1. Results

##### 3.1.1. AAO-directed 1D TiO<sub>2</sub> nanotubes

Fig. 1(a) shows the XRD patterns from two AAO templates coated with 500 ALD cycles under 150 (as marked with “A”) and 250 °C (as

marked with “B”). Apparently, the one at 150 °C displays no XRD peaks while the one at 250 °C exhibits many sharp XRD peaks which are consistent to the reference values for the crystalline anatase TiO<sub>2</sub> (JCPDS PDF No. 21-1272). The XRD patterns imply that growth temperature took effect on the ALD-TiO<sub>2</sub>. To confirm the success of ALD-TiO<sub>2</sub> at 150 °C, EDS was employed to probe elemental compositions of an ALD-coated AAO template which was partially etched by NaOH, as shown in Fig. 1(b). It was revealed that there is plenty of Ti, as well as O, Na, and Al. Besides Ti due to ALD-TiO<sub>2</sub>, the oxygen element can be ascribed to some remained AAO as well as ALD-induced coatings at 150 °C. Al is due to the sample holder of aluminum and AAO, while Na should be incurred by the etching of NaOH. Obviously, temperatures played critical roles in the ALD-TiO<sub>2</sub>, and the low temperature of 150 °C might have contributed to the growth of amorphous TiO<sub>2</sub>. In Fig. 1(c), Raman spectra of the two samples are shown. The sample A at 150 °C displays some weak features comprising two very broad and weak bands in the vicinity of 170 and 610 cm<sup>-1</sup>. These features have been previously observed and assigned to the amorphous phase of TiO<sub>2</sub> [53]. In contrast, the sample B at 250 °C shows a very strong peak around 144 cm<sup>-1</sup> and some weak peaks at 399, 519, and 639 cm<sup>-1</sup> as well. These peaks are typically assigned to the anatase TiO<sub>2</sub> [53–55].

To further address the growth characteristics induced by different temperatures, the coated AAO samples were examined by

SEM and TEM. Fig. 2(a) and (b) shows SEM images for the cross sections of 500- and 600-cycle coated AAO at 150 °C, respectively. Each of them reveals a smooth and uniform layer deposited in AAO nanopores, accounting for 16.7 and 20.5 nm in thickness, respectively. Through etching AAO with a 0.5 M NaOH solution, nanotube arrays were received for each case, i.e. 500- (Fig. 2(c)) and 600-cycle (Fig. 2(d)) ALD-TiO<sub>2</sub>, respectively. It was noticed that the received nanotubes exhibit fluffy structures in their inner surfaces, as signified by red arrows in Fig. 2(d) and inset of Fig. 2(d). We postulated that it might be due to the amorphous nature of the nanotubes vulnerable to the NaOH solution, leading to the deposited material to partially peel off in the forms of thin strips. Fig. 2(e) shows the TEM image of received nanotubes after 500 ALD cycles and shows some fluctuation in wall thickness along the tubes. It further confirms that the amorphous phase of TiO<sub>2</sub> is easily subject to the influence of NaOH etching processes. The inset of Fig. 2(e) shows the selected area electron diffraction (SAED) patterns which disclose a disordered nature of the deposited material. This is consistent to the XRD data in Fig. 1. The HR-TEM image in Fig. 2(f) also discloses the amorphous nature of a local area (as denoted in Fig. 2(e) with “f”).

Fig. 3 shows the growth characteristics of ALD-TiO<sub>2</sub> at 250 °C. Fig. 3(a)–(c) jointly disclose that the wall thickness increases from 8.7 to 17.9 and 35.3 nm with ALD-cycles increased from 200 (Fig. 3(a)), to 300 (Fig. 3(b)) and 500 (Fig. 3(c)). It was noticed that the inner surfaces of the received nanotubes are smooth and free of fluffy structures as observed in Fig. 2. Fig. 3(d) presents the SEM image of some bunches of the received nanotubes. In Fig. 3(e), the received nanotubes are displayed by a TEM image and the SAED pattern in the inset reveals their polycrystalline nature. Fig. 3(f) unveils the structural characteristics of the nanotube walls (the inset indicates the examined location of the nanotube) with a HR-TEM image, clearly showing the lattices of anatase TiO<sub>2</sub>. The inter-plane distances of 0.352 and 0.243 nm correspond to the characteristic planes of (101) and (104) of anatase TiO<sub>2</sub>, respectively.

### 3.1.2. CNT-based 1D TiO<sub>2</sub> coaxial nanotubes

In the above section, we demonstrated the growth characteristics of AAO template-directed ALD-TiO<sub>2</sub>. In another route, ALD-TiO<sub>2</sub> was deposited on oxidized CNTs and the following section discusses the results based on the CNTs of 1 h oxidation. Fig. 4(a) shows the XRD patterns for CNTs (as marked with “A”), ALD-coated CNTs at 150 °C (as marked with “B”), and the ones at 250 °C (as marked with “C”). Compared to the XRD pattern (A) of CNTs, the pattern of ALD-TiO<sub>2</sub> coated CNTs at 150 °C (B) shows no changes, implying the amorphous nature of the deposited TiO<sub>2</sub>. In contrast, the XRD pattern for ALD-coated CNTs at 250 °C (C) displays many peaks as marked and they are consistent to the reference values for the crystalline anatase TiO<sub>2</sub> (JCPDS PDF No. 21-1272). Fig. 4(b) shows the Raman spectra of the three samples. The sample A disclosed the features of CNTs comprising G (1580 cm<sup>-1</sup>) and D (1330 cm<sup>-1</sup>) band [56]. Besides the features of CNTs, the sample B and C revealed the amorphous and anatase TiO<sub>2</sub> phase (as discussed in the above case of AAO), respectively. Again, it is confirmed that growth temperatures took part in determining the growth of ALD-TiO<sub>2</sub>, as revealed in the section 3.1.1.

To further examine the growth characteristics of TiO<sub>2</sub> on CNTs, both SEM and TEM were applied. The ALD-TiO<sub>2</sub> on CNTs at 150 °C is shown in Fig. 5. After 100 cycles, SEM (Fig. 5(a)) and TEM (Fig. 5(b)) image jointly show that some tiny particles of less than 10 nm were deposited on CNTs. Increasing the cycling number to 200 cycles, SEM (Fig. 5(c)) and TEM (Fig. 5(d)) image combine to reveal that a very thin layer of around 4.5 nm was deposited on CNTs. Further increasing the cycling number to 300 cycles, it was found that the deposited film became thicker. As shown by the SEM image of Fig. 5(e), the broken part (as circled by a yellow dashed line) exposed that a uniform film covers CNTs. TEM image of Fig. 5(f)

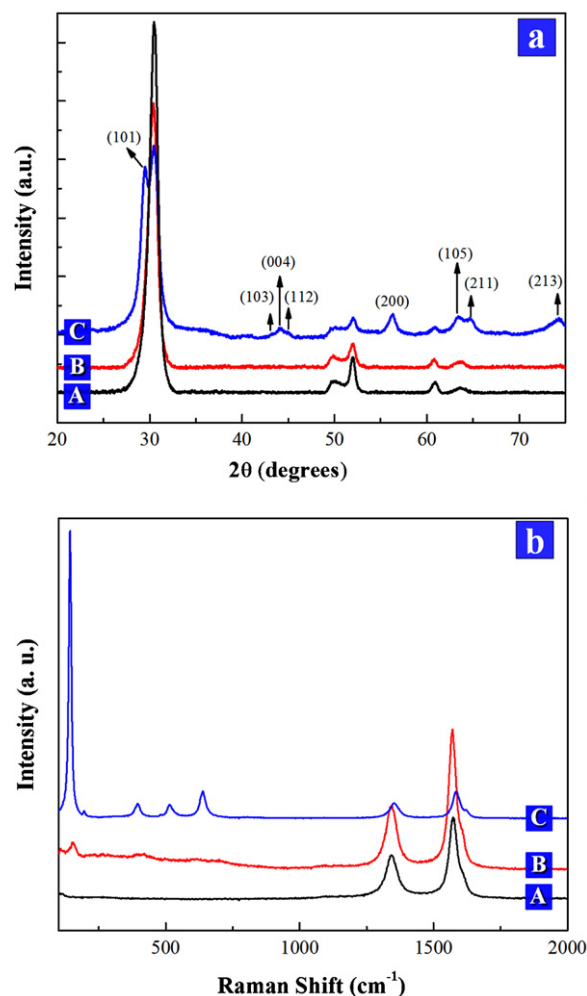


Fig. 4. (a) XRD patterns of (A) pristine CNTs, and 300-cycle ALD-TiO<sub>2</sub> on CNTs at (B) 150 and (C) 250 °C. (b) Raman spectra of (A) pristine CNTs, and 300-cycle ALD-TiO<sub>2</sub> on CNTs at (B) 150 and (C) 250 °C.

shows that the film thickness is 8.6 nm. Furthermore, a CNT sample coated with 100-cycle TiO<sub>2</sub> was examined by HR-TEM, as shown in Fig. 5(g). It clearly shows the graphitic lattices of CNT walls, accounting for an inter-plane distance of 0.34 nm. In addition, as surrounded by yellow dashed lines, the disordered nature of the deposited material is displayed.

Fig. 6 illustrates the growth characteristics of ALD-TiO<sub>2</sub> on CNTs at 250 °C. The morphological changes due to 100-, 200-, and 300-cycle ALD-TiO<sub>2</sub> are shown by SEM images in Fig. 6(a), (c), and (e), respectively. They jointly reveal that the surfaces of coated CNTs are rough. Fig. 6(b) exposes that there are numerous nanoparticles of around 10 nm deposited on CNTs, which were going to coalesce. The inset of Fig. 6(b) further reveals that the nanoparticles are crystalline with identified lattices, as marked for the planes of (200). Upon the finishing of 200 cycles, Fig. 6(d) shows that nanoparticles coalesced into an average 7.7 nm thick film. As shown by Fig. 6(f), the films grew thickened to 12.1 nm after 300 cycles.

### 3.2. Discussions

In the above sections, experimental results clearly demonstrated that ALD resulted in two distinct nanostructures of TiO<sub>2</sub>, i.e., pure TiO<sub>2</sub> nanotubes and CNTs-TiO<sub>2</sub> coaxial tubular hybrids, ascribed to the two distinct substrates of AAO and CNTs. In addition, it is also easy to conclude that the resultant TiO<sub>2</sub> is subject

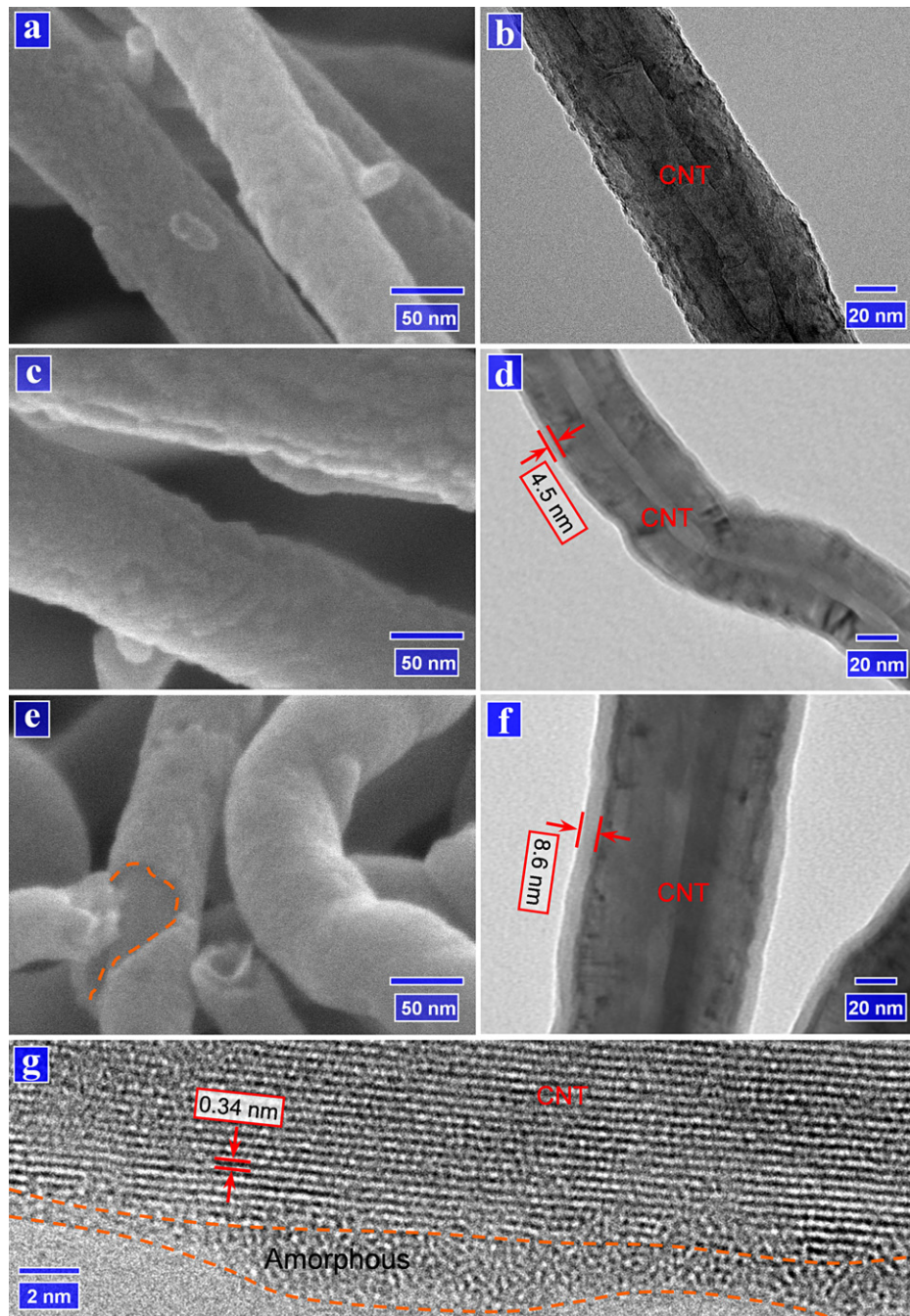


**Fig. 5.** ALD-TiO<sub>2</sub> on CNTs at 150 °C. SEM images of (a) 100, (c) 200, and (e) 300 cycles of ALD-TiO<sub>2</sub>. TEM images of (b) 100, (d) 200, and (f) 300 cycles of ALD-TiO<sub>2</sub>. (g) HR-TEM image of 100-cycle ALD-TiO<sub>2</sub>.

to the influences of both temperatures and substrates, leading to controllable structural phases and tunable morphologies. To clarify these facts, we make further discussions in the following sections, especially based on effects of temperatures and substrates.

### 3.2.1. Effects of substrates

In any ALD process, the behaviors of film growth are jointly determined by three key parameters, i.e., precursors, temperatures, and substrates [57]. It is apparent that, with the use of TTIP and water in this study, temperatures and substrates are the two factors responsible for the resultant ALD-TiO<sub>2</sub>.

As is well known, ALD is a surface-controlled process. Thus, the initiation and the subsequent deposition of an ALD process are closely related with the surface nature of applied substrates. It was

previously reported that, using TiCl<sub>4</sub> and water as ALD precursors, amorphous TiO<sub>2</sub> films were grown on glasses while crystalline films were deposited on crystalline substrates at the same conditions [58]. Similarly, Schuisky et al. also demonstrated that substrates could influence the structural phases of as-deposited TiO<sub>2</sub> using TiI<sub>4</sub> and H<sub>2</sub>O<sub>2</sub> as ALD precursors [59]. However, this study disclosed no difference on structural phases of the resultant TiO<sub>2</sub> when the same temperature was applied. Thus, it is reasonable to believe that the substrates in this study are not the critical factors for the formation of amorphous and crystalline anatase TiO<sub>2</sub>. Even so, we did observe some difference on GPC of ALD-TiO<sub>2</sub>. At 150 °C the average GPC of ALD-TiO<sub>2</sub> is 0.34 and 0.29 Å/cycle for AAO and CNTs, respectively. At 250 °C, the average GPC of ALD-TiO<sub>2</sub> is 0.71 and 0.40 Å/cycle for AAO and CNTs, respectively. Obviously, the growth

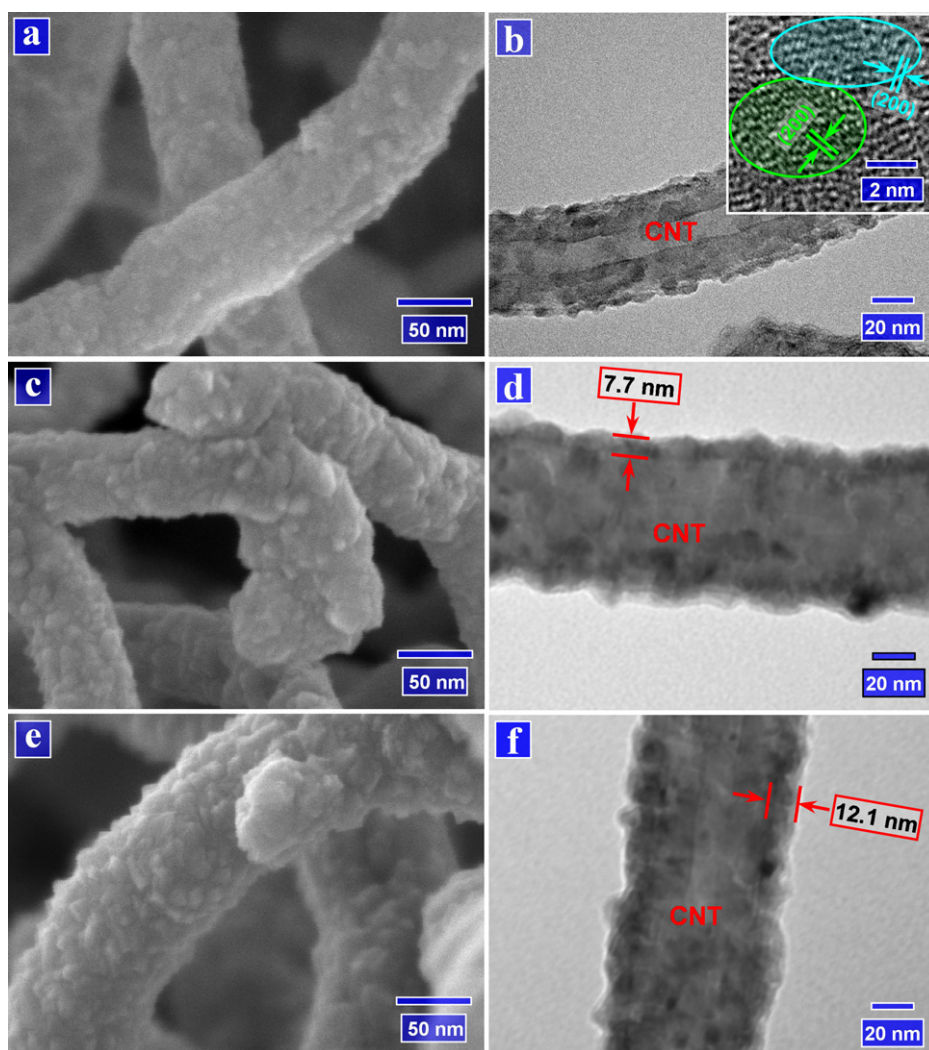


**Fig. 6.** ALD-TiO<sub>2</sub> on CNTs at 250 °C. SEM images of (a) 100, (c) 200, and (e) 300 cycles of ALD-TiO<sub>2</sub>. TEM images of (b) 100 (inset: HR-TEM image of nanoparticles), (d) 200, and (f) 300 cycles of ALD-TiO<sub>2</sub>.

on AAO is higher than the one on CNTs. The reason is probably due to the higher density of reactive sites with AAO in comparison to CNTs. In this way, our previous studies well demonstrated that AAO can be used directly for ALD processes [47] while CNTs need pre-functionalization prior to an ALD process [51]. In addition, we also compared the ALD-TiO<sub>2</sub> based on 1 h (see Fig. 5 and 6) and 2 h (see Fig. SI-2) oxidized CNTs, and there is no evident difference observed from the two treated CNTs. This might be ascribed to the slow oxidization process via HNO<sub>3</sub>, which needs further investigation in future work. However, the island-growth mode of ALD-TiO<sub>2</sub> (see Fig. 5(b) and 6(b)) exposes a low density of reactive sites.

### 3.2.2. Effects of temperatures

Besides substrates, temperatures can also play critical roles in ALD processes. On the choice of temperatures, it is in essence determined by the fundamentals of ALD as well as the properties of precursors. As a layer-by-layer deposition technique, ALD requires that precursors will not decompose by themselves under a given growth temperature [32,60]. Otherwise, the deposition will be a process of chemical vapor deposition (CVD), and destroy the self-limiting growth mechanism of ALD. Of the two precursors (TTIP and water), water being an oxygen source has been used for ALD under a temperature up to 600 °C [58] and could not be an issue. The limit is mainly from TTIP. Some pioneered work conducted by Finnish researchers [32–34] has disclosed that TTIP is only chemically

stable under a temperature of 250 °C or less. In other words, any higher temperature would incur an increasing part of CVD growth of TiO<sub>2</sub> due to the decomposition of TTIP. In this work, it is obvious that the two temperatures of 150 and 250 °C are safe for ALD-TiO<sub>2</sub>.

With growth temperature increased from 150 to 250 °C, the ALD-TiO<sub>2</sub> on both AAO and CNTs changed distinctively from the amorphous to crystalline anatase phase. The two substrates are by nature structurally different. AAO is amorphous while CNTs are crystalline. Thus, the results imply that growth temperatures played dominant roles other than the substrates in determining the structures of as-deposited TiO<sub>2</sub>. Similarly, Aarik et al. also revealed that higher temperatures are preferable to the growth of crystalline films on silicon substrates during ALD-TiO<sub>2</sub> of using TiCl<sub>4</sub> and water as precursors [58]. Similarly, Liu et al. reported that, using TiCl<sub>4</sub> and water as ALD-TiO<sub>2</sub> precursors, a high temperature of 400 °C resulted in anatase nanotubes while a low temperature of 100 °C produced amorphous nanotubes [26]. In this study, temperature could take effect by two ways. On one hand, a higher temperature (250 °C) should be kinetically favorable for the ordering of the structure with minimum energy [58], for the intermediates might be able to migrate easily and enable the Ti and/or O ions to occupy the positions corresponding to the lowest free energy of the crystal. On the other hand, temperature can influence GPC through changing the reactions between precursors and surface-reactive sites. The potential mechanism may lie in the improved reactivity due

to the increased temperature. Aarik et al. [33] revealed that water has a low reactivity toward TTIP in the ALD-TiO<sub>2</sub>, but an increase on growth temperature could improve the reactivity of water, activate some reactions, and thereby improve the growth rate of ALD-TiO<sub>2</sub>. In comparison to the study of Li et al. [26], it is apparent that the temperature of 250 °C in this study is much lower than their temperature of 400 °C for crystalline anatase TiO<sub>2</sub> nanotubes, accounting for the influence of precursors. In other words, this study provided a route to tune the crystallinity of TiO<sub>2</sub> nanotubes from amorphous to anatase phase with low growth temperatures (below 250 °C). This is especially important for heat-sensitive substrates such as polymer and biological materials.

To further address the transformation of TiO<sub>2</sub> from amorphous to crystalline phase with increased temperatures, we investigated the deposition on AAO at an intermediate temperature of 200 °C, where a mixed growth of amorphous and crystalline TiO<sub>2</sub> was observed (see Fig. SI-3). As revealed by Fig. SI-3(a) and (b), the deposition at 200 °C is nearly linear and the GPC is around 0.5 Å/cycle. Fig. SI-3(c) shows the TEM image of 200-cycle TiO<sub>2</sub> nanotubes. The netlike walls were likely induced by the ultrasound used in the sample preparation. We did not use the ultrasound for the TEM samples in Fig. 2, otherwise there were no samples survived for TEM observation. It is worth noting that the SAED patterns in Fig. SI-3(c) disclose some weak polycrystalline characteristic. HR-TEM image in Fig. SI-3(d) further reveals that the walls are mostly amorphous while many small crystals (as red-cycled) have formed after a 200-cycle ALD-TiO<sub>2</sub> at 200 °C. Thus, there is a competitive growth between amorphous and crystalline TiO<sub>2</sub> at 200 °C. Fig. SI-3(e) compares the XRD patterns of 500-cycle ALD-TiO<sub>2</sub> on AAO, due to the three temperatures (i.e., 150, 200, and 250 °C). It confirms that the ALD-TiO<sub>2</sub> at 200 °C shows some crystalline characteristics, but its crystallinity is obviously much weaker than the one at 250 °C. These temperature-dependent crystallinity and growth have also been observed in our previous work [44–47], and they have given more detailed explanations.

In summary, this study worked on fabrication of ALD-TiO<sub>2</sub> for different 1D nanostructures using two different substrates. It is found that both substrates and temperatures are important influencing factors which make the deposited TiO<sub>2</sub> controllable in both structural phases and morphologies.

#### 4. Conclusions

In this work, we attempted to fabricate 1D nanotubes and CNT-based core-shell structures of TiO<sub>2</sub>. It was demonstrated that ALD is a highly tunable technique in controlling the deposited TiO<sub>2</sub> in different morphologies and phases. First, depending on the adopted temperature, the ALD-TiO<sub>2</sub> on both AAO and CNTs can be tuned from the amorphous to crystalline anatase phase in the range of 150–250 °C. Furthermore, the deposited TiO<sub>2</sub> can be morphologically controlled by adjusting cycling numbers. In addition, the two substrates exhibited some influence on GPC of ALD-TiO<sub>2</sub> due to their difference on surface nature. The resultant nanostructured TiO<sub>2</sub> is useful for many applications such as water splitting, solar cells, lithium-ion batteries, and gas sensors.

#### Acknowledgements

This research was supported by the Natural Science and Engineering Research Council of Canada (NSERC), Canada Research Chair (CRC) Program, Canadian Foundation for Innovation (CFI), Ontario Research Fund (ORF), Early Researcher Award (ERA) and the University of Western Ontario. In addition, the authors would like to appreciate the help from Mr. Fred Pearson on HRTEM analysis at Canadian Center for Electron Microscopy, McMaster University.

#### Appendix A. Supplementary data

Supplementary data associated with this article can be found, in the online version, at <http://dx.doi.org/10.1016/j.apsusc.2012.11.116>.

#### References

- [1] S. Iijima, *Nature* 354 (1991) 56.
- [2] M. Lee, T.W. Kim, C. Bae, H. Shin, J. Kim, *JOM* 62 (2010) 44.
- [3] Y.-C. Nah, I. Paramasivam, P. Schmuki, *ChemPhysChem* 11 (2010) 2698.
- [4] J. Zhu, M. Zäch, *Current Opinion in Colloid and Interface Science* 14 (2009) 260.
- [5] G.K. Mor, O.K. Varghese, M. Paulose, K. Shankar, C.A. Grimes, *Solar Energy Materials and Solar Cells* 90 (2006) 2011.
- [6] D.V. Bavykin, J.M. Friedrich, F.C. Walsh, *Advanced Materials* 18 (2006) 2807.
- [7] M. Adachi, J. Jiu, S. Isoda, *Current Nanoscience* 3 (2007) 285.
- [8] K. Rajeshwar, *Journal of Applied Electrochemistry* 37 (2007) 765.
- [9] C. Aprile, A. Corma, H. Garcia, *Physical Chemistry Chemical Physics* 10 (2008) 769.
- [10] D.V. Bavykin, F.C. Walsh, *European Journal of Inorganic Chemistry* 8 (2009) 977.
- [11] Z. Yang, D. Choi, S. Kerisit, K.M. Rosso, D. Wang, J. Zhang, G. Graff, J. Liu, *Journal of Power Sources* 192 (2009) 588.
- [12] K. Shankar, J.I. Basham, N.K. Allam, O.K. Varghese, G.K. Mor, X. Feng, M. Paulose, J.A. Seabold, K.-S. Choi, C.A. Grimes, *Journal of Physical Chemistry C* 113 (2009) 6327.
- [13] A. Ghicov, P. Schmuki, *Chemical Communications* (2009) 2791.
- [14] W. Zhou, H. Liu, R.I. Boughton, G. Du, J. Lin, J. Wang, D. Liu, *Journal of Materials Chemistry* 20 (2010) 5993.
- [15] D.P. Singh, N. Ali, *Science of Advanced Materials* 2 (2010) 295.
- [16] Z. Su, W. Zhou, *Journal of Materials Chemistry* 21 (2011) 8955.
- [17] G. Zhang, S. Finefrock, D. Liang, G.G. Yadav, H. Yang, H. Fang, Y. Wu, *Nanoscale* 3 (2011) 2430.
- [18] D. Gong, C.A. Grimes, O.K. Varghese, W. Hu, R.S. Singh, Z. Chen, E.C. Dickey, *Journal of Materials Research* 16 (2001) 3331.
- [19] H. Shin, D.-K. Jeong, J. Lee, M.M. Sung, J. Kim, *Advanced Materials* 16 (2004) 1197.
- [20] C.J.W. Ng, H. Gao, T.T.Y. Tan, *Nanotechnology* 19 (2008) 445604.
- [21] L.K. Tan, M.A.S. Chong, H. Gao, *Journal of Physical Chemistry C* 112 (2008) 69.
- [22] G.-M. Kim, S.-M. Lee, G.H. Michler, H. Roggendorf, U. Gösele, M. Knez, *Chemistry of Materials* 20 (2008) 3085.
- [23] J. Lee, H. Ju, J.K. Lee, H.S. Kim, J. Lee, *Electrochemistry Communications* 12 (2010) 210.
- [24] J.T. Korhonen, P. Hiikkataipale, J. Malm, M. Karppinen, O. Ikkala, R.H.A. Ras, *ACS Nano* 5 (2011) 1967.
- [25] Y.-C. Liang, C.-C. Wang, C.-C. Kei, Y.-C. Hsueh, W.-H. Cho, T.-P. Perng, *Journal of Physical Chemistry C* 115 (2011) 9498.
- [26] C.-M. Liu, C. Chen, H.-E. Cheng, *Journal of the Electrochemical Society* 158 (2011) K58.
- [27] T. Suntola, J. Antson, U.S. Patent 1977 4058430.
- [28] M. Knez, K. Nielsch, L. Niinistö, *Advanced Materials* 19 (2007) 3425.
- [29] H. Kim, H.B.R. Lee, W.J. Maeng, *Thin Solid Films* 517 (2008) 2563.
- [30] S.M. George, *Chemical Reviews* 110 (2010) 111.
- [31] X. Meng, X.-Q. Yang, X. Sun, *Advanced Materials* 24 (2012) 3589.
- [32] M. Ritala, M. Leskelä, *Chemistry of Materials* 5 (1993) 1174.
- [33] J. Aarik, A. Aidla, T. Uustare, M. Ritala, M. Leskelä, *Applied Surface Science* 161 (2000) 385.
- [34] A. Rahtu, M. Ritala, *Chemical Vapor Deposition* 8 (2002) 21.
- [35] Q. Xie, Y.L. Jiang, C. Detavernier, D. Deduytsche, R.L. Van Meirhaeghe, G.P. Ru, B.Z. Li, X.P. Qu, *Journal of Applied Physics* 102 (2007) 083521.
- [36] A. Suisalu, J. Aarik, H. Mändar, I. Sildos, *Thin Solid Films* 336 (1998) 295.
- [37] J. Aarik, A. Aidla, H. Mändar, V. Sammelselg, *Journal of Crystal Growth* 220 (2000) 531.
- [38] R. Matero, A. Rahtu, M. Ritala, *Chemistry of Materials* 13 (2001) 4506.
- [39] R. Methaapanon, S.F. Bent, *Journal of Physical Chemistry C* 114 (2010) 10498.
- [40] G.K. Hyde, S.M. Stewart, G. Scarel, G.N. Parsons, C.-C. Shih, C.-M. Shih, S.-J. Lin, Y.-Y. Su, N.A. Monteiro-Riviere, R.J. Narayan, *Biotechnology Journal* 6 (2011) 213.
- [41] J.D. Ferguson, A.R. Yoder, A.W. Weimer, S.M. George, *Applied Surface Science* 226 (2004) 393.
- [42] D.M. King, X. Liang, Y. Zhou, C.S. Carney, L.F. Hakim, P. Li, A.W. Weimer, *Powder Technology* 183 (2008) 356.
- [43] X.D. Wang, E. Graugnard, J.S. King, Z.L. Wang, C.J. Summers, *Nano Letters* 4 (2004) 2223.
- [44] X. Meng, D. Geng, J. Liu, R. Li, X. Sun, *Nanotechnology* 22 (2011) 165602.
- [45] X. Meng, D. Geng, J. Liu, M. Banis, Y. Zhang, R. Li, X. Sun, *Journal of Physical Chemistry C* 114 (2010) 18330.
- [46] X. Meng, Y. Zhong, Y. Sun, M.N. Banis, R. Li, X. Sun, *Carbon* 49 (2011) 1133.
- [47] X. Meng, Y. Zhang, S. Sun, R. Li, X. Sun, *Journal of Materials Chemistry* 21 (2011) 12321.
- [48] K. Le Van, H. Groult, A. Mantoux, L. Perrigaud, F. Lantelme, R. Lindström, R. Badour-Hadjean, S. Zanna, D. Lincot, *Journal of Power Sources* 160 (2006) 592.
- [49] J.W. Diggle, T.C. Downie, C.W. Goulding, *Chemical Reviews* 69 (1969) 365.

- [50] G. Xiong, J.W. Elam, H. Feng, C.Y. Han, H.-H. Wang, L.E. Iton, L.A. Curtiss, M.J. Pellin, M. Kung, H. Kung, P.C. Stair, *Journal of Physical Chemistry B* 109 (2005) 14059.
- [51] X. Meng, M. Ionescu, M.N. Banis, Y. Zhong, H. Liu, Y. Zhang, S. Sun, R. Li, X. Sun, *Journal of Nanoparticle Research* 13 (2011) 1207.
- [52] Z. Wang, M.D. Shirley, S.T. Meikle, R.L.D. Whitby, S.V. Mikhailovsky, *Carbon* 47 (2009) 73.
- [53] A. Niilisk, M. Moppel, M. Pärs, I. Sildos, T. Jantson, T. Avarmaa, R. Jaaniso, J. Aarik, *Central European Journal of Physics* 4 (2006) 105.
- [54] M.J. Šćepanović, M. Grujić-Brojčin, Z.D. Dohčević-Mitrović, Z.V. Popvić, *Science of Sintering* 41 (2009) 67.
- [55] N. Mahdjoub, N. Allen, P. Kelly, V. Vishnyakov, *Journal of Photochemistry and Photobiology A* 211 (2010) 59.
- [56] P. Delhaes, M. Couzi, M. Trinquocoste, J. Dentzer, H. Hamidou, C. Vix-Guterl, *Carbon* 44 (2006) 3005.
- [57] R.L. Puurunen, *Journal of Applied Physics* 97 (2005) 121301.
- [58] M. Ritala, M. Leskelä, E. Nykänen, P. Soininen, L. Niinistö, *Thin Solid Films* 225 (1993) 288.
- [59] M. Schuisky, A. Harsta, A. Aidla, K. Kukli, A.A. Kiisler, J. Aarik, *Journal of the Electrochemical Society* 147 (2000) 3319.
- [60] M. Leskelä, M. Ritala, *Angewandte Chemie International Edition* 42 (2003) 5548.